Simulated Performances of a Very High Energy Tomograph for Non-Destructive Characterization of large objects

Marc Kistler, Nicolas Estre and Elsa Merle

***Abstract*— As part of its R&D activities on high-energy X-ray imaging for non-destructive characterization, the Nuclear Measurement Laboratory has started an upgrade of its imaging system currently implemented at the CEA-Cadarache center. The goals are to achieve a sub-millimeter spatial resolution and the ability to perform tomographies on very large objects (more than 100-cm standard concrete or 40-cm steel). This paper presents results on the detection part of the imaging system.**

The upgrade of the detection part needs a thorough study of the performance of two detectors: a series of CdTe semiconductor sensors and two arrays of segmented $CdWO_4$ scintillators with different pixel sizes. This study consists in a Quantum Accounting Diagram (QAD) analysis coupled with Monte-Carlo simulations. The scintillator arrays are able to detect millimeter details through 140 cm of concrete, but are limited to 120 cm for smaller ones. CdTe sensors have lower but more stable performance, with a 0.5 mm resolution for 90 cm of concrete. The choice of the detector then depends on the preferred characteristic: the spatial resolution or the use on large volumes. The combination of the features of the source and the studies on the detectors gives the expected performance of the whole equipment, in terms of signal-over-noise ratio (SNR), spatial resolution and acquisition time.

***Index Terms*—CdTe, $CdWO_4$, detective quantum efficiency (DQE), high-energy imaging, quantum accounting diagram (QAD), signal-over-noise ratio (SNR), tomography.**

I. Introduction

As PART of its R&D activities on high-energy imaging for non-destructive characterization, the Nuclear Measurement Laboratory is working on the upgrade of the tomograph implemented at the CEA-Cadarache Center. This upgrade takes into account the optimization of the detection system. That is why two different types of detectors are studied: a series of CdTe semiconductor sensors and two arrays of segmented $CdWO_4$ scintillators with different pixel sizes.

The comparison of the detectors is carried out by three indicators: the detective quantum efficiency (DQE), the spatial resolution and the signal-over-noise ratio (SNR). The DQE and the spatial resolution make it possible to compare the intrinsic performance of the detectors. The DQE can be calculated theoretically using parameters derived from a Quantum Accounting Diagram (QAD) analysis. The spatial resolution of the detector, relative to the object plane, gives the component of the tomograph spatial resolution due to the detection part. Coupled with a X-ray source (up to 20 MeV in the current studies), it allows to evaluate the spatial resolution of the complete system. The signal-over-noise ratio, on the other hand, depends on the DQE, but also on the input X-ray flux and on the acquisition time (the flux being determined by the source and the object to be imaged). The acquisition time depends in part on the type of detector used and the associated technique (horizontal scan or fixed object).

The goal is therefore to obtain a sub-millimeter spatial resolution, while keeping a significant SNR at the output of the detector, in order to obtain images with sufficient contrast and limited noise.

II. Detectors Description and QAD Analysis

The QAD analysis of a detector consists in representing its detection process as a series of cascaded stages of three types: gain stage, spread stage and additive noise stage [1]. This precise and standardized representation allows accurate comparisons and analyses of several detection systems at each stage of the detection process.

A. Multi-CdTe Detector

In the 1990s, the CEA-Leti has designed a detector based on a series of 25 CdTe sensors, separated by lead collimators and followed by an electronic acquisition chain [2]. This device still shows remarkable intrinsic performances [3].

Each sensor consists of a thin CdTe semiconductor lamella with a section of 0.8 mm x 15 mm. Its thickness of 25 mm and its high density ($\rho = 5.8$ g / cm^3) allow to capture at least 40% of the incident photons (Fig. 3). Photons deposit an amount of energy during the interaction, leading to the production of

This paragraph of the first footnote will contain the date on which you submitted your paper for review.

M. Kistler and N. Estre are with CEA Cadarache, DEN/Nuclear Measurement Laboratory, F-13108 Saint-Paul-lez-Durance, France (e-mail: marc.kistler@cea.fr).

E. Merle is with CNRS, IN2P3/Subatomic Physics and Cosmology Laboratory, F-38026 Grenoble, France.

Fig. 1. Multi-CdTe detector, with the collimators [3].

TABLE I
SUMMARY OF THE GAINS AND POISSON EXCESSES FOR THE STAGES OF THE CDTE DETECTOR

#	Description	Type of process	Symbol	Gain g_i	Poisson excess ε_{g_i}
1	X-ray interaction	Binomial gain	g_1	0.399	-0.399
2	X/Deposited energy conversion (MeV/ph-X)	Gain	g_2	1.72	-0.446
3	Energy spread in the sensor	Spread	$T_3(\omega)$	1	-1
4	Conversion in e^-/e^+ pairs	Gain	g_4	2.31×10^5	-0.85
5	Electrons collection	Binomial gain	g_5	0.78	-0.78
6	Additive electronic noise	Noise	$\sigma_a^2/\overline{N_6}$	1	-1

electron-hole pairs. The voltage created at the output of the integrator circuit is proportional to the number of collected charges. The QAD analysis is in this case composed of six stages, summarized in Table I. See reference [1] for the parameters definition.

Since the sensors are non-continuous, the complete acquisition of a tomographic section requires a translation of the object, in addition to its rotation and a precise synchronization of the acquisition with the object displacement and the firing frequency of the X-ray source. This results in an acquisition time per tomographic slice close to 30 min.

B. Segmented $CdWO_4$ Scintillator Array

The company X-Scan Imaging offers a series of linear X-ray cameras. These detectors are composed of segmented $CdWO_4$ scintillator, forming needles, coupled by optical taper to an off-axis linear matrix of photodiodes. The two models studied, XIH8804-66 and XIH8808-66, differ in the size of their needles, with a section of 0.4 mm × 0.6 mm and 0.8 mm × 1.2 mm respectively. With an ideal active detection length of 1.7 m and respectively 4224 and 2112 pixels, theses detectors allow measurements in half-field on objects with a 140 cm diameter without having to translate the object.

The detection process combines a high-density scintillator material (ρ = 7.9 g/cm^3) and therefore a high X-ray interaction efficiency, with small continuous pixels. The QAD analysis consists of seven stages. The values have been evaluated by simulations (parameters 1 to 5) or realistic assumptions (parameters 6 and 7).

Fig. 3 and 4 show that both detectors have an equivalent interaction efficiency higher than 40% and that each photon deposits an energy of a few MeV. Due to its small section, the $CdWO_4$ 0.4 model has the lowest energy deposition values.

Fig. 2. Segmented $CdWO_4$ scintillator [4].

TABLE II
SUMMARY OF THE GAINS AND POISSON EXCESSES FOR THE STAGES OF THE $CDWO_4$ DETECTOR

#	Description	Type of process	Symbol	Gain g_i	Poisson excess ε_{g_i}
1	X-ray interaction	Binomial gain	g_1	0.436	-0.436
2	X/Deposited energy conversion (MeV/ph-X)	Gain	g_2	0.85 / 1.55	-0.71 / -0.61
3	Energy spread in the needles	Spread	$T_3(\omega)$	1	-1
4	Conversion to optical quanta (ph/MeV)	Gain	g_4	1.50×10^4	0
5	Optical fiber efficiency	Binomial gain	g_5	0.31	-0.31
6	Quantum efficiency of the photodiodes	Binomial gain	g_6	0.48	-0.48
7	Additive electronic noise	Noise	$\sigma_a^2/\overline{N_7}$	1	-1

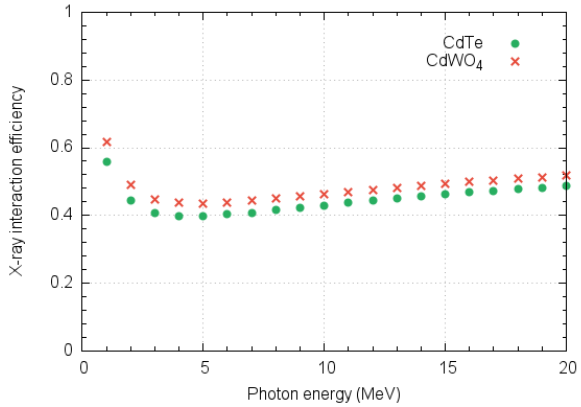

Fig. 3. X-ray interaction efficiency g_1 of each detector as a function of incident photon energy.

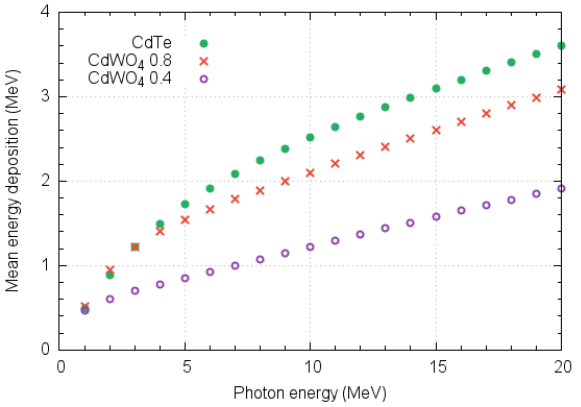

Fig. 4. Mean single interaction energy deposition g_2 of each detector as a function of incident photon energy.

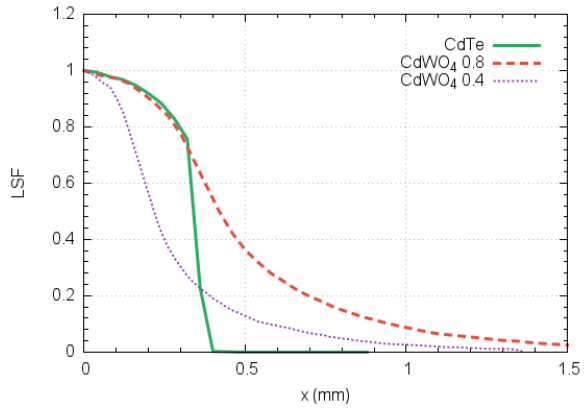

Fig. 5. Line Spread Function (LSF) of each detector.

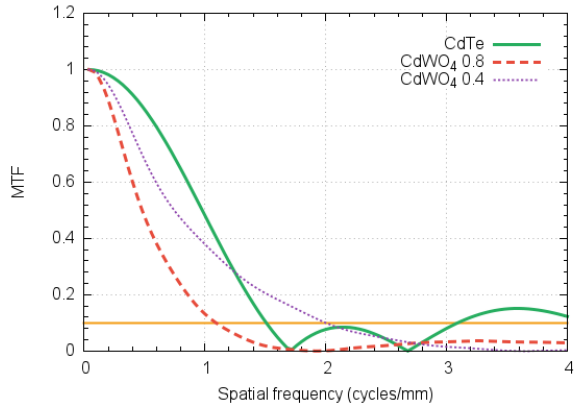

Fig. 6. Modulation Transfer Function (MTF) of each detector.

III. Results

A. Spatial Resolution and MTF

The spreading stages are materialized by the effect of signal spreading on the average number of quanta. This effect is directly characterized by the square of the Modulation Transfer Function (MTF) [1]. In order to evaluate the MTF, we first calculate the Line Spread Function (LSF), which is the one-dimension signal spread distribution. In this study, the LSF is evaluated by Monte-Carlo simulation (code MCNP6.1 [5]). The MTF is then obtained by Fourier Transform of the LSF and can be included in the QAD calculations.

The MTF also provides the resolution limit that we define as the spatial frequency at which the MTF is 10%. Beyond this frequency, it is considered that the signal is not exploitable. The LSF and MTF obtained for the two detectors are shown in Fig. 5 and 6 respectively.

The LSF of the CdTe detectors is close to a sensor width rectangular function, thanks to the lead collimation. $CdWO_4$ arrays have more complex distributions, with a fine central part and a wider peripheral part, which reflects the spreading of the signal due to the absence of collimation. The resolution limit of the small $CdWO_4$ needles remains better than the CdTe one in spite of a larger signal spreading. The large $CdWO_4$ needles (which have the same width as the CdTe sensors) have the poorest resolution.

Finally, the resolution limits are calculated in the object plane of the tomograph via the radiographic magnification factor, which is 1.6 for our setup. These values are summarized in Table III.

TABLE III
Resolution limits in detector and object planes for each detector

	$CdWO_4$ 0.4	CdTe	$CdWO_4$ 0.8
Detector plane	2 mm^{-1}	1.5 mm^{-1}	1 mm^{-1}
Object plane	3.2 mm^{-1}	2.4 mm^{-1}	1.6 mm^{-1}

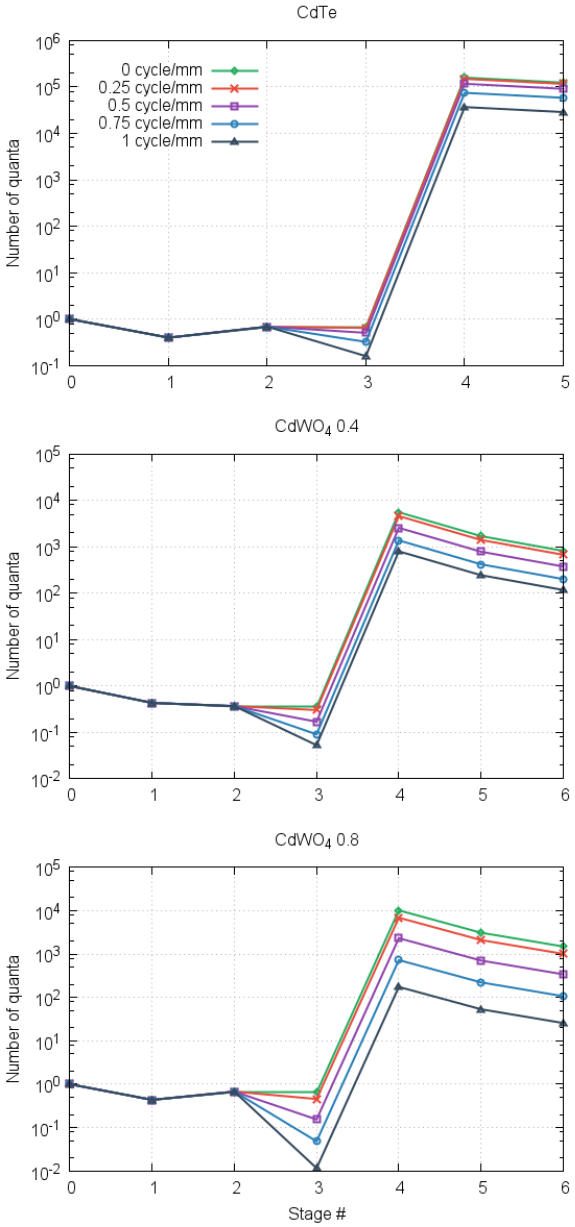

Fig. 7. Spatial-frequency dependent QAD of each detector.

B. QAD

As QAD parameters are evaluated, the diagrams can then be computed (Fig. 7). For the three detectors, they represent the evolution of the number of quanta $P_i(\omega)$ at each detection stage i and for different spatial frequencies ω:

$$P_i(\omega) = \prod_{j=1}^{i} \overline{g_j} \left|T_j(\omega)\right|^2 \quad (1)$$

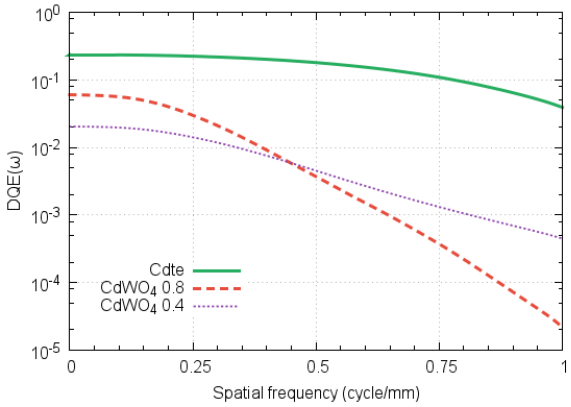

Fig. 8. Intrinsic Detective Quantum Efficiency (DQE) of each detector.

The diagrams show that the detection processes are equivalent: first a loss of signal in the first stage, then a spreading that appears through the separation of the curves according to the spatial frequencies, followed by a significant gain of several decades, and finally a small decrease due to the electrons or visible photons collecting efficiency. The larger separation of the curves for the large $CdWO_4$ suggests a higher sensitivity of its DQE to the spatial frequency.

C. DQE

The formulas of the DQE for each detector are obtained from the theoretical equation [6]. The three curves are plotted in Fig. 8.

$$\text{CdTe: } DQE(\omega) = \frac{g_1 g_2 |T_3(\omega)|^2}{1+(g_2+\epsilon_{g_2})|T_3(\omega)|^2+\frac{\epsilon_{g_4}}{g_4}+\frac{1+\sigma_a^2/N_6}{g_4 g_5}} \quad (2)$$

$$\text{CdWO}_4\text{: } DQE(\omega) = \frac{g_1 g_2 |T_3(\omega)|^2}{1+(g_2+\epsilon_{g_2})|T_3(\omega)|^2+\frac{1+\sigma_a^2/N_7}{g_4 g_5 g_6}} \quad (3)$$

CdTe sensors have the best intrinsic DQE over the entire frequency range. The $CdWO_4$ is more frequency dependent and therefore drops faster, especially the large one after 0.5 cycle/mm.

IV. Discussion

For a single incident photon, multi-CdTe detector is therefore the most efficient. But for the acquisition of a tomographic slice with an identical measurement time, it is necessary to compare the signal-over-noise ratios at the output of the detectors. Indeed, the SNR depends not only on the DQE, but also on the SNR at the detector input:

$$SNR_{out} = \sqrt{DQE} \times SNR_{in} \quad (4)$$

The input SNR depends on the photonic flux, the sensors section and the acquisition time of the signal per sensor. These last two values differ between each detector, and can counterbalance a low DQE, finally delivering a readable SNR to the detector output. Fig. 9 shows the output SNR of each detector as a function of the equivalent thickness of concrete imaged with a nominal flux of 10^6 X / mm² / pulse, for spatial

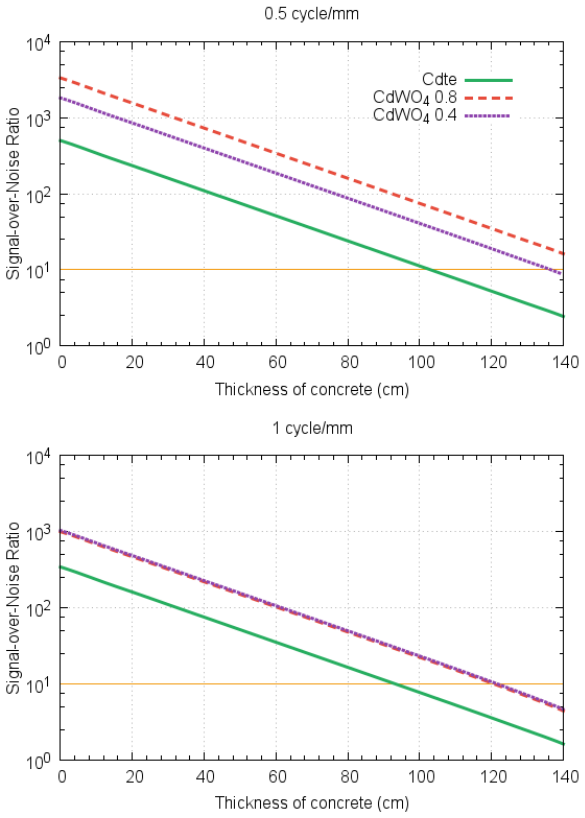

Fig. 9. Output Signal-over-Noise Ratio (SNR) of each detector as a function of the thickness of concrete, for 0.5 and 1 cycle/mm.

frequencies of 0.5 and 1 cycle/mm.

The readability of an image is arbitrarily fixed for a minimum SNR of 10. With the CdTe detector, it is possible in this setup to discern details up to the millimeter scale (0.5 cycle/mm) in a 100 cm thick concrete block, and sub-millimeter details through 90 cm of concrete (1 cycle/mm). For $CdWO_4$, the millimeter resolution is reached for 140 cm of concrete, with better performance for the large needles. Both models have a 500 µm resolution across 120 cm.

Finally, we should notice that the resolution limits discussed above are first approximations because the real limits will depend in the first place on the contrasts offered by the objects inspected at this level of detail. Taking into account these levels of contrasts is beyond the scope of this study and will be characterized later on and verified experimentally.

V. Conclusion

This study of two possible detectors for high energy tomography reveals notable performance, in terms of spatial resolution as well as penetration capacity. It appears that the multi-CdTe detector has the best intrinsic performance, with a relatively stable DQE, which provides a SNR that is slightly spatial frequency dependent and therefore spatial resolution dependent. For an equal acquisition time, the linear $CdWO_4$ scintillator arrays have a better SNR input, which counterbalances their lower DQE and results in a higher output SNR.

Thanks to the pixel size, the small model of $CdWO_4$ has the

best spatial resolution; the large model and the multi-CdTe detector have a lower resolution. In parallel, a practical asset of the $CdWO_4$ scintillator is the large width of the detector that dispenses with the transverse displacement of the object. However, reaching a sub-millimeter resolution with a penetration capacity of 140 cm of concrete seems to be difficult.

This study by QAD analysis will be completed by an experimental verification in order to compare *in situ* the performance of the detectors.

REFERENCES

[1] J.-P. Bissonnette *et al., "*A quantum accounting and detective quantum efficiency analysis for video-based portal imaging," *Med. Phys.,* vol. 24, no. 6, pp. 815-826, Jun. 1997.

[2] F. Glasser *et al., "*Application of cadmium telluride detectors to high energy computed tomography," *Nucl. Instrum. Methods Phys. Res. A,* vol. 322, pp. 619-622, Nov. 1992.

[3] N. Estre *et al., "*High-energy X-ray imaging applied to nondestructive characterization of large nuclear waste drums," in *IEEE Transactions on Nuclear Science,* vol. 62, no. 6, pp. 3104-3109, Dec. 2015.

[4] X-Scan Imaging Corporation, XI880 X-ray LDA. Available: https://x-scanimaging.com/cammods/xi8800/, Accessed on: May 16, 2017.

[5] Los Alamos National Laboratory, "MCNP6 Users Manual - Code Version 6.1," Jun. 2014.

[6] I. A. Cunningham *et al., "*A spatial-frequency dependent quantum accounting diagram and detective quantum efficiency model of signal and noise propagation in cascading imaging systems," *Med. Phys.,* vol. 21, no. 3, pp. 417-427, Mar. 1994.